water

MDPI

Article

Comparison of Long-Term Changes in Non-Linear Aggregated Drought Index Calibrated by MERRA–2 and NDII Soil Moisture Proxies

Fhumulani Mathivha [1,*] and Nkanyiso Mbatha [2,*]

[1] Department of Earth Sciences, University of Venda, Thohoyandou 0950, South Africa
[2] Department of Geography and Environmental Studies, University of Zululand, KwaDlangezwa 3886, South Africa
* Correspondence: fhumulani.mathivha@univen.ac.za or fhumulani.mathivha@icloud.com (F.M.); mbathanb@unizulu.ac.za (N.M.)

Abstract: This study aimed at evaluating Modern-Era Retrospective Analysis for Research and Applications, Version 2 (MERRA–2) and Normalized Difference Infrared Index (NDII) soil moisture proxies in calibrating a comprehensive Non-linear Aggregated Drought Index (NADI). Soil moisture plays a critical role in temperature variability and controlling the partitioning of water into evaporative fluxes as well as ensuring effective plant growth. Long-term variability and change in climatic variables such as precipitation, temperatures, and the possible acceleration of the water cycle increase the uncertainty in soil moisture variability. Streamflow, temperature, rainfall, reservoir storage, MERRA–2, and NDII soil moisture proxies' data from 1986 to 2016 were used to formulate the NADI. The trend analysis was performed using the Mann Kendall, SQ-MK was used to determine the point of trend direction change while Theil-Sen trend estimator method was used to determine the magnitude of the detected trend. The seasonal correlation between the NADI-NDII and NADI-MERRA–2 was higher in spring and autumn with an R^2 of 0.9 and 0.86, respectively. A positive trend was observed over the 30 years period of study, NADI-NDII trend magnitude was found to be 2.94 units per year while that of NADI-MERRA–2 was 1.21 units. Wavelet analysis showed an in-phase relationship with negligible lagging between the NDII and MERRA–2 calibrated NADI. Although a robust comparison is recommended between soil moisture proxies and observed soil moisture, the soil moisture proxies in this study were found to be useful in monitoring long-term changes in soil moisture.

Keywords: drought; drought indices; evaporation; soil moisture; SQ-MK; trends analysis; water resources; wavelet analysis

Citation: Mathivha, F.; Mbatha, N. Comparison of Long-Term Changes in Non-Linear Aggregated Drought Index Calibrated by MERRA–2 and NDII Soil Moisture Proxies. *Water* **2022**, *14*, 26. https://doi.org/10.3390/w14010026

Academic Editor: Hossein Tabari

Received: 9 November 2021
Accepted: 13 December 2021
Published: 23 December 2021

1. Introduction

Climate change is expected to alter precipitation, temperature and increase the probability of occurrence of extreme events such as heatwaves, sea surface temperature, and droughts amongst others. Drought hazards are considered relative rather than absolute condition because they found in both high and low rainfall areas [1]. Studies such as [1,2] reported that droughts are characterised by slow-onset hazards and a slow, gradually creeping phenomenon. The latter phenomenon is defined as an extended period, either seasonal or annual where an area receives below-average rainfall [2]. Globally, drought frequency, severity and durations are reported to have been increasing [1]. For the case of the Limpopo River Basin, it lies between 20° and 25°, and [3] reported that countries located between these latitudes in southern Africa are in a drought corridor, which makes them prone to dry spells. The severity of drought is being aggravated by the rise in water demand and global climate change [4], putting water supplies and agricultural production and consequently food security at risk [2]. In disciplines, such as atmospheric science and agriculture, dynamics of soil moisture in the root zone of vegetation is essential, since this part of the vadose zone is the core component controlling the partitioning of water into

evaporative fluxes, drainage, recharge, and runoff [5]. Soil moisture is generally driven by climate, particularly precipitation and temperature [6]. Precipitation is the main source of soil moisture, while temperature affects soil moisture by controlling evapotranspiration [7]. Long-term changes in climatic variables such as precipitation and temperatures driven by a warming planet and the potential acceleration of the water cycle increase the uncertainty in soil moisture variability [8,9] further stated that reduced soil water levels are typically associated with soil water stress for vegetation, which constitutes a major constraint on the physiological functioning of natural and cultivated ecosystems and which can thus lead to large impacts on agricultural production. For the case of developing countries, community's livelihoods are greatly dependent on agriculture, while drought events can have devastating impacts, leading to famine, migration, and potential conflict [10].

For long-term drought monitoring and assessment, different drought quantifying parameters are used, however, drought indices have been used as drought quantifying parameters. The Standardised Precipitation Index (SPI) [11], Standardised Precipitation Evaporation Index (SPEI) [12], Normalised Difference Vegetation Index (NDVI) [13], Palmer Drought Severity Index (PDSI) [14], Surface Water Index (SWI) [15], Aggregate Drought Index (ADI) [16] among others have been applied extensively in drought studies. Since drought exhibits multi-dimensional characteristics and influenced by several factors [17–19] indicated that a simple index that depends on one variable to define drought (i.e., SPI) is often faced with challenges in capturing drought onset. For a comprehensive picture of catchment drought, an index that considers most or all components of the hydrological cycle is more useful. Indices such as Aggregated Drought Index (ADI), and Non-linear Aggregated Drought Index (NADI), [20] and consider all components of the hydrological cycle. Soil moisture is a required variable in the formulation of ADI, PDSI, NADI. This parameter is considered important since it governs the partitioning of the mass and energy fluxes between the terrestrial system in land-atmosphere interactions [21,22], thus playing a key role in the assessment of the different components of the water and energy balance [23].

Long-term observed soil moisture data are sparse in many developing countries because of the cost associated with monitoring. Thus, indirect methods are often used to monitor and quantify soil moisture. Physically based and land surface models provide estimates of soil moisture [24] while certain drought indices are also used as a proxy of soil moisture [12,25]. Computational improvement of flow through two and three-dimensional heterogeneous soils was reported through a combination physically-based Extended Cellular Automata model and asynchronism strategy by [26]. The Richards' equation has been successfully applied in modelling studies to model movement in unsaturated soils [27]. However, an analytical solution of Richards' equation is complex as it depends on the peculiar choice of hydraulic functions and boundary conditions [28]. Ref. [26] also indicated that due to the nature of hydrological modelling, the application of physically-based models at the catchment scale is limited due to intensive calculation requirements. Therefore, it is for this reason that the current study proposes to apply a soil moisture proxy approach.

Several remote sensing products have been developed for monitoring soil moisture (e.g., SMOS, ERS, and AMSR-E) but until now correlations between remote sensing products and observed soil moisture at different depths have been modest at best [29]. The NDII is widely used to monitor the equivalent water thickness of leaves and canopy [30]. While comparing NDII with a lumped conceptual model, Ref. [5] illustrated the potential of the NDII as a proxy for catchment-scale root zone moisture deficit. The MERRA–2; Ref. [31] is the first long-term global reanalysis to assimilate space-based observations of aerosols and represent their interactions with other physical process in the climate system. On the MERRA–2 land surface hydrology estimates assessment study, Ref. [32] showed that MERRA–2 and MERRA-Land have the highest surface and root zone soil moisture skill, slightly higher than that of ERA-Interim/Land and higher while being validated against in situ measurements from over 300 stations in North America, Europe, and Australia. This study, therefore, aims to formulate a long-term NADI calibrated with MERRA-2 root zone

soil moisture and NDII as a soil moisture proxy. The selected soil moisture proxies are also compared for their performance in soil moisture estimations as utilised in this study.

2. Materials and Methods

2.1. The Study Area

The Luvuvhu River Catchment (LRC) study site is located between latitudes 22°17′33.57″ S and 23°17′57.31″ S and longitudes 29°49′46.16″ E and 31°23′32.02″ E in Limpopo Province in north eastern part of South Africa, shown in Figure 1. The LRC covers an area of approximately 5941 km^2 with topography ranging between 198 m and 1450 m above sea level.

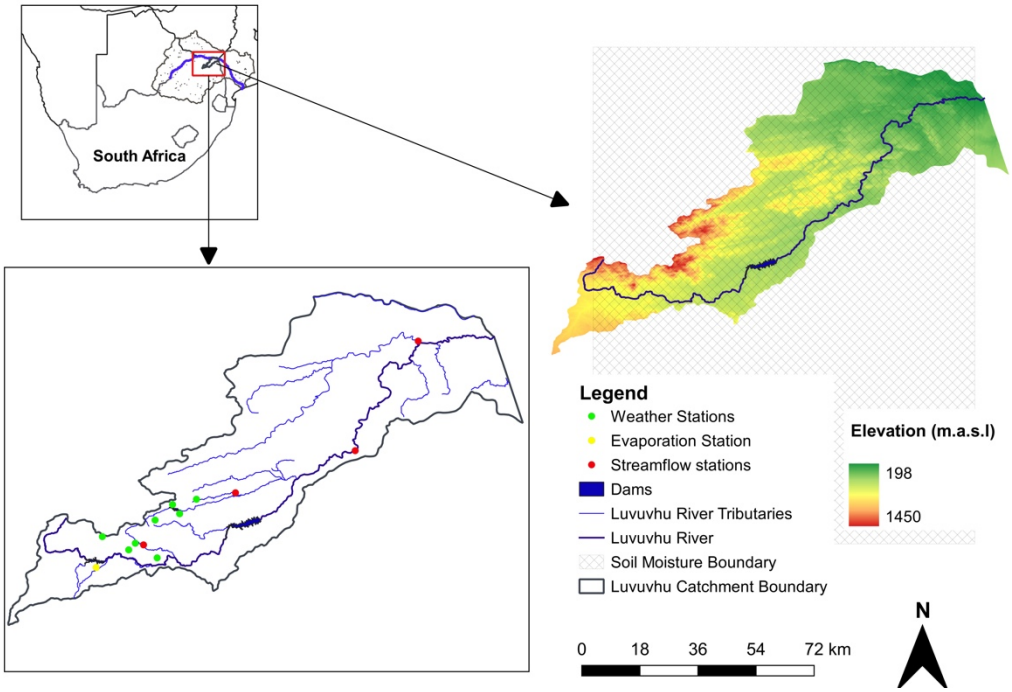

Figure 1. The study area, Luvuvhu River Catchment.

The nature of the catchment's topography influences rainfall distribution with the highest rainfall received in the upper reaches while the lower reaches around the Kruger National park receiving the lowest rainfall during the wet season. The distribution of rainfall through the year shows a highly seasonal characteristic with 95% of the rainfall occurring during the summer months (October and March). The upper reaches Mean Annual Precipitation (MAP) is approximately 1800 mm/annum with hotter areas in the Lowveld receiving precipitation of 400 mm/year. The overall mean annual rainfall of the catchment is 608 mm and the mean annual run-off is 520 × 10^6 m^3 [33]. Areas that experience lower rainfall occurrence in the catchment tend to experience greater variability than the higher rainfall areas. In this area, temperature increases from the mountains in the west part to the lower reaches in the east part of the catchment. In terms of meteorology, local towns such as Thohoyandou experience daily temperatures that range approximately 25 °C to 40 °C in summer and between 22 °C and 26 °C in winter months [34]. The study area is dominantly rural, with a community that is highly dependent on commercial and subsistence agriculture.

2.2. Datasets and Data Pre-Processing

Data requirements for the computation of NADI in the LRC included; rainfall (weather stations: Mukumbani, Klein Australie, Matiwa, Nooitgedatch, Levubu, Vondo Bos, Shefera, and Tshivhase), evaporation (station A9E002), streamflow (stations: A9H003 and A9H006, A9H012 and A9H013), reservoir storage volume (Vondo Dam), soil moisture data. Monthly

data for 30 hydrological years spanning from 1986 to 2016 were considered for the study. Figure 1 shows the location of rain gauges, reservoirs, weather station, and streamflow within the catchment. Table 1 shows the location, elevation, and mean data for the respective datasets used in the study. Daily minimum and maximum temperatures from three weather stations (Levubu, Mukumbani, and Tshivhase stations) were collected from SAWS.

Table 1. Location and other characteristics of the respective datasets used in the study.

	Station Name	Location		Elevation m.a.s.l	Mean
		Latitude	Longitude		
Rainfall	Mukumbani	−22.9169	30.4055	762	82.32 mm
	Klein Australie	−23.05	30.22	702	97.72 mm
	Matiwa	−22.98	30.28	1311	147.25 mm
	Nooitgedatch	23.07	30.2	762	78.65 mm
	Levubu	−23.0798	30.28	706	66.08 mm
	Vondo Bos	−22.933	30.333	1130	111.27 mm
	Shefera	−23.03	30.12	1214	103.68 mm
	Tshivhase	−22.9607	30.3545	976	120.77 mm
Temperature	Mukumbani	−22.9169	30.4055	762	20.512 °C
	Levubu	−23.0798	30.28	706	19.643 °C
	Tshivhase	−22.9607	30.3545	976	21.154 °C
Evaporation	A9E002	−23.124	30.105	801	112.459 mm
Streamflow	A9H003	−22.898	30.5238	554	2.4214 m/s
	A9H006	−23.0357	30.2775	693	10.502 m/s
	A9H012	−22.7685	30.8893	428	82.456 m/s
	A9H013	−22.4377	31.0778	258	81.474 m/s

Note: m.a.s.l—meters above sea level, mm—millimeters, °C—degree Celsius, m/s—meters per second.

Due to lack of ETo data in the study area, Hargreaves and Samani temperature-based method [35] was applied to temperature data to estimate PET Equation (1):

$$ET_o = 0.0023(T_{max} - T_{min})^{0.5}(T + 17.8)R_a \quad (1)$$

where ET_o is the reference evapotranspiration, R_a is the extraterrestrial radiation in $mm.day^{-1}$, T_{max} and T_{min} are the maximum temperature and minimum temperature, respectively, in degrees Celsius. Root zone soil moisture was considered for this study because it plays a significant role in the regulation of water and energy budgets at the soil–vegetation–atmosphere interface through evaporation processes of the uppermost surface soil layer and plant transpiration [36]. The root zone soil moisture data was obtained from the NASA earth data Giovanni repository. The Modern-Era Retrospective analysis for Research and Applications version 2 (MERRA–2) Model data was selected as it had data for the study area for the period considered in this study. MERRA–2 is a NASA atmospheric reanalysis for the satellite era using the Goddard Earth Observing System Model, Version 5 (GEOS-5) with its Atmospheric Data Assimilation System (ADAS), version 5.12.4. Monthly root zone soil moisture time series from September 1986 to August 2016 were obtained from the Giovanni repository from the bounding box (Figure 1) at 0.5° × 0.625° spatial resolution. The normalized difference infrared index (NDII) covering the LRC, was computed using MODIS bands 2 and 6 reflectance data. The index has been proven to be a good representation of root-zone soil moisture and has been widely applied around the world [5,37] including South Africa [38]. NDII was computed using Equation (2):

$$NDII = \frac{NIR - SWIR1}{NIR + SWIR1} \quad (2)$$

where NIR and SWIR1 are the near infrared (700–1300 nm) and shortwave infrared (1550–1750 nm), respectively.

2.3. NADI Formulation for the Luvuvhu River Catchment

NADI for the LRC was formulated using five hydro-meteorological variables (i.e., precipitation, evapotranspiration, streamflow, reservoir storage volume and soil moisture content). The two NADI time series were developed based on MERRA–2 and NDII soil moisture indicators. The formulation of NADI steps followed in this study was adapted from [39] as shown in Figure 2. NADI was used as a drought indicator and threshold values were calculated probabilistically for the study area using an empirical CDF. The SPI threshold was used to generate the NADI threshold, SPI dryness threshold is Gaussian variates −2, −1.5, −1 and 1 standard deviations which correspond to the 2.3rd, 6.7th, 16.0th and 84.0th percentiles in the SPI cumulative distribution. The NADI threshold corresponding to the latter percentiles for the LRC were −2.05, −1.42, −1.09 and 1.01 respectively.

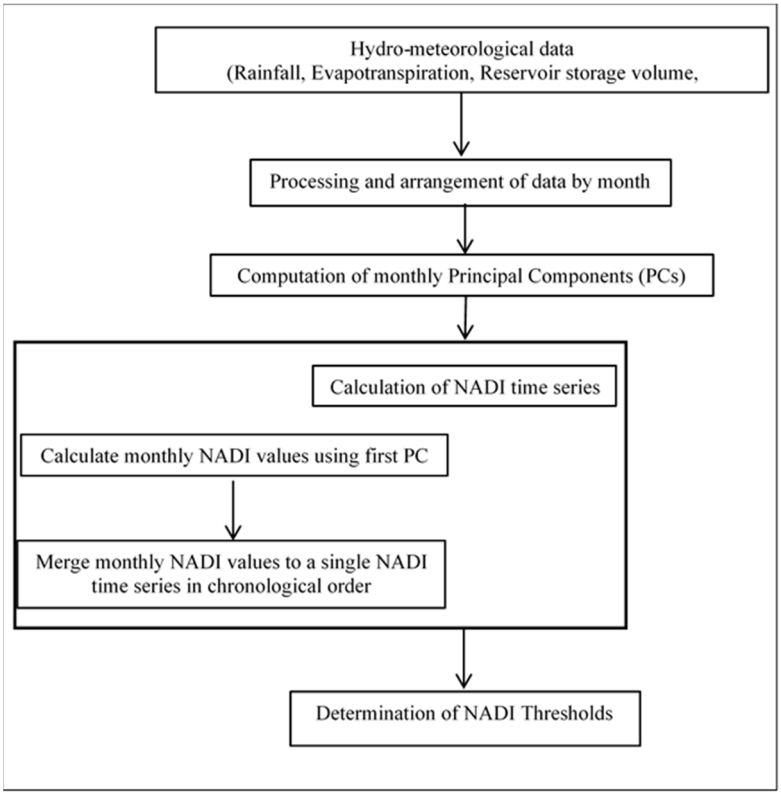

Figure 2. Formulation of the Non-linear Aggregated Drought Index flowchart (Source; [20]).

2.4. Drought Statistical Analysis

2.4.1. Variable of Importance

To determine the variables importance of climate indices (i.e., PSDI, SPI, DMI, Rainfall temperature and El Nino 3.4) influences on drought as depicted by NADI, random forest (RF) was used. In random forests, an ensemble of classification trees is created by means of drawing several bootstrap samples or subsamples from the original training data and fitting a single classification tree to each sample [40]. The latter further stated that because of random variation in the samples and the instability of the single classification trees, the ensemble will consist of a diverse set of trees. The accuracy of the RF model used in this research was improved by factors such as tuning parameters to optimise RF performance, the number of features, and also by using the classical method of splitting the input data into training and testing. This also assists to avoid over-fitting in the random forest model. During the partitioning of data, 70% was used as training data, and 30% was used as the testing part of the model. During the experiment design, the number of decision trees in the model was a primary consideration. For purpose of the selection of the optimum range

of the decision trees, the experimental design of this research utilized out-of-bag error, and the misclassification error. The main function of the out-of-bound error method is to measure prediction error using bootstrap sampling to subsample data that did not appear for training [41]. A procedure for RF model performance and also avoiding over-fitting is outlined in a study by [42], in their study on hyperparameter optimisation of machine learning algorithms. More details about the RF model experimental design used in this research is explained in detail in [43]. Improved prediction accuracy of ensembles is realised by means of smoothing the hard-cut decision boundaries created by splitting in single classification trees, thereby reducing the variance of the prediction. This has been shown by empirical studies [44,45] and theoretical results [46].

2.4.2. Trend Analysis

For the purpose of this study, the Breaks for Additive Seasonal and Trend (BFAST) (see Equation (3)) method was applied to decompose the drought index time series to obtain the trend variations in the study area. The BFAST method can be mathematically represented as:

$$y_t = m + T_t + S_t + R_t \tag{3}$$

where m is the mean, T is the trend component value, S is the seasonal component, and R is the random component at the time step t. On the other hand, this study aimed to investigate the trend in the NADI time series. Thus, the monotonic trends in the NADI time series was obtained through the use of the Mann–Kendall (MK) non-parametric trend test. Based on a study by [47–51] amongst others, the MK test statistic is calculated from the following equations:

$$S = \sum_{k=1}^{n-1} \sum_{j=k+1}^{n} \operatorname{sign}(X_j - X_k) \tag{4}$$

$$\operatorname{sign}(x) = \begin{cases} 1 & x_j > x_i \\ 0 & x_j = x_i \\ -1 & x_j < x_i. \end{cases} \tag{5}$$

The average value of S is E[S] = 0 and the variance σ^2 is given by the following equation:

$$\sigma^2 = \frac{\left\{ n(n-1)(2n+5) - \sum_{j=1}^{p} t_j (t_j - 1)(2t_j + 5) \right\}}{18} \tag{6}$$

where t_j is the number of data points in the *j*th tied group. The parameter p represents the number of the tied group in the time series. The summation operator used in the above equation is applied only in the case of tied groups in the time series. This operator is used to reduce the influence of individual values in tied groups in the ranked statistics. On the assumption of random and independent time series, the statistic S is approximately normally distributed if the following z-transformation equation is used:

$$Z = \begin{cases} \frac{S-1}{\sigma} & S > 0 \\ 0 & S = 0 \\ \frac{S+1}{\sigma} & S < 0. \end{cases} \tag{7}$$

The value of the S statistic is associated with the Kendall expression:

$$\tau = \frac{S}{D} \tag{8}$$

where:

$$D = \left[\frac{1}{2} n(n-1) - \frac{1}{2} \sum_{j-1}^{p} t_j (t_j - 1) \right]^{1/2} \left[\frac{1}{2} n(n-1) \right]^{1/2} \tag{9}$$

Regarding the z-transformation equation defined above, this research opted to employ a 5% confidence level statistic, where the null hypothesis of no trend was rejected if $|z| > 1.96$. Moreover, the MK statistics is the Kendall τ term, which is a measure of correlation that indicates the strength of the relationship between any two independent variables was also considered important in this study. The MK test system summarized above was applied to the NADI time series data by writing a code in R-project and following the instructions given by [52]. studies involving animals or humans, and other studies that require ethical approval, must list the authority that provided approval and the corresponding ethical approval code.

2.4.3. Sequential Mann-Kendall Test and Theil-Sen Trend Estimator

Another special form of the Mann-Kendal test method is the sequential version of the Mann–Kendall test statistic which is called the Sequential Mann–Kendall (SQ-MK). This method was proposed by [53], and its main purpose is to detect approximate potential trends turning points in long-term time series. The output of this method is two-time series, namely, a progressive (u(t)) (forward) and a retrograde (u'(t)) (backwards). For effectiveness utilization of this trend detection method, it is required that both the progressive and the retrograde time series are plotted in the same figure. If they happen to cross each other and diverge beyond the specific threshold (± 1.96 in this study), then there is a considered as a statistically significant trend in the time series. Those regions where they cross each other indicate the time period where the trend turning point begins [54]. This method is computed by using ranked values of y_i of a given time series (x_1,x_2, x_3, ..., x_n) in the analyses. The magnitudes of y_i, (i = 1, 2, 3, ..., n) are compared with y_i, (j = 1, 2, 3, ..., j − 1). At each comparison, the number of cases where $y_i > y_j$ are counted and then donated to n_i. The statistic t_i is mathematically defined by the following equation:

$$t_i = \sum_{j=1}^{i} n_i \tag{10}$$

The mean and variance of the statistic t_i are given by:

$$E(t_i) = \frac{i(i-1)}{4} \tag{11}$$

and:

$$Var(t_i) = \frac{i(i-1)(2i-5)}{72} \tag{12}$$

Finally, the sequential values of statistic $u(t_i)$, which are standardized, are calculated using the following equation:

$$u(t_i) = \frac{t_i - E(t_i)}{\sqrt{Var(t_i)}} \tag{13}$$

The above equation gives a forward sequential statistic which is normally called the progressive statistic. To calculate the backward/retrograde statistic values (u'(t)), the same time series (x_1, x_2, x_3, ..., x_n) is used, however, statistic values are calculated by starting from the end of the time series. The combination of the forward and backward sequential statistic allows for the detection of the approximate beginning of a developing trend [51]. Additionally, in this study, a 95% confidence level was considered, which means critical limit values are ± 1.96. This method has been successfully utilized in studies of trends detection in temperature and precipitation [55,56]. Further to the MK and SQ-MK, the Theil-Sen trend methodology was used to the slope of the trend for both NADI-NDII and NADI-MERRA–2. The Theil-Sen line is a nonparametric alternative to the parametric ordinary least squares' regression line. An ordinary least squares regression line models how the mean concentration changes linearly with time; a Theil-Sen line models how the median (50th percentile) concentration changes linearly with time. The Theil-Sen

method [57,58], which is based on Kendall's rank correlation, is used to estimate trends and is commonly used in combination with the Mann-Kendall test to provide both an estimate and a test for trend [59]. The Theil-Sen method considers measurements Y_1, Y_2, Y_3, ..., Y_n of an environmental variable (say the concentration of a pollutant) taken at times t_1, t_2, t_3,..., t_n, where $t_1 \leq t_2 \leq t_3 \leq ... \leq t_n$ (the time intervals do not necessarily have to be equal), as independent observations. The gradient D_k, (k = 1, 2, 3, ..., N), for each N pairs of observations taken at times t_j and t_i such that $1 \leq i \leq j \leq n$ and $(t_j - t_i) > 0$, can be calculated as:

$$D_k = (Y_j - Y_i)/(t_j - t_i) \tag{14}$$

The estimate of trend ($\hat{\beta}$) in the data series Y_1, Y_2, Y_3, ..., Y_n can then be calculated as:

$$\hat{\beta} = \begin{cases} D_{(\frac{N-1}{2})+1} & \text{if N is odd,} \\ \frac{D_{\frac{N}{2}} + D_{(\frac{N}{2})+1}}{2} & \text{if N is even.} \end{cases} \tag{15}$$

The above represents an empirical nonparametric calculation of the median of D_k. The $(1 - \alpha)$ confidence interval for $\hat{\beta}$ may be calculated as follows:

(1) Compute M1 and M2 using the estimate (Vs) from the MK test described above and the $(1 - \alpha/2)$ quantile of the standard normal distribution ($_{(1-\alpha/2)}$) as:

$$M_1 = \frac{(N - Z)_{(1-\alpha 2)} V_s}{2} \text{ and } M_2 = \frac{(N + Z)_{(1-\alpha 2)} V_s}{2} \tag{16}$$

(2) Determine the order statistics D_{M1} and D_{M2+1} as the lower and upper $(1 - \alpha)$ confidence limits respectively from the collection of the N gradients (D_k).

2.5. Wavelet Analysis

For the purpose of this research, the Morlet wavelet family was used for analysing periodicities that are contained in the time series. The advantage of this method is that it provides a good balance between time and frequency localization [60]. Wavelet analysis includes different wavelet functions such as the windowed Fourier Transform, wavelet transform, normalization, wavelet power spectrum, etc. One of the main advantages of wavelet analysis in comparison with other techniques is that it analyses localised variations of power within a time series. Wavelet transform coherence has the capability of analysing the coherence and phase lag between two time-series with the time and frequency. Therefore, this study adopted the Morlet Carlo wavelet and coherence analysis to quantify the relationship between NADI-NDII and NADI-MERRA–2. More information on the wavelet analysis applied in this study can be obtained [60,61]. The Wavelet analysis method helps to determine the dominant modes of variability and their variation with time.

3. Results

3.1. Exploratory Data Analysis

Table 2 shows the statistics of the 30 years of NADI-NDII and NADI-MERRA-2 time series for the period considered in this study. The NADI-NDII and NADI-MERRA–2 showed the variance of 0.972 and 0.969 respectively. Most of the kurtosis values for indices were found to be much smaller while the skewness was reported as 0.082 and 0.041. Normally distributed data produces a skewness of zero with possibilities of small variations [62]. The skewness results obtained in this study by both indices suggest that the data is approximately asymmetrical. Although [62] suggested that a skewness statistic of 0.01819 was acceptable for normally distributed data, skewness ranging between −0.5 and 0.5 is still considered acceptable and fairly asymmetrical. For further distribution analysis, density and violin plots were generated and are shown in Figure 3a,b. From these plots, NADI-MERRA–2 is distribution is seen to be smoother compared to NADI-NDII. Therefore, NADI-MERRA–2 is normally distributed while NADI-NDII is showing that the data is characterised by a bimodal distribution. It should provide a concise and precise description

of the experimental results, their interpretation, as well as the experimental conclusions that can be drawn.

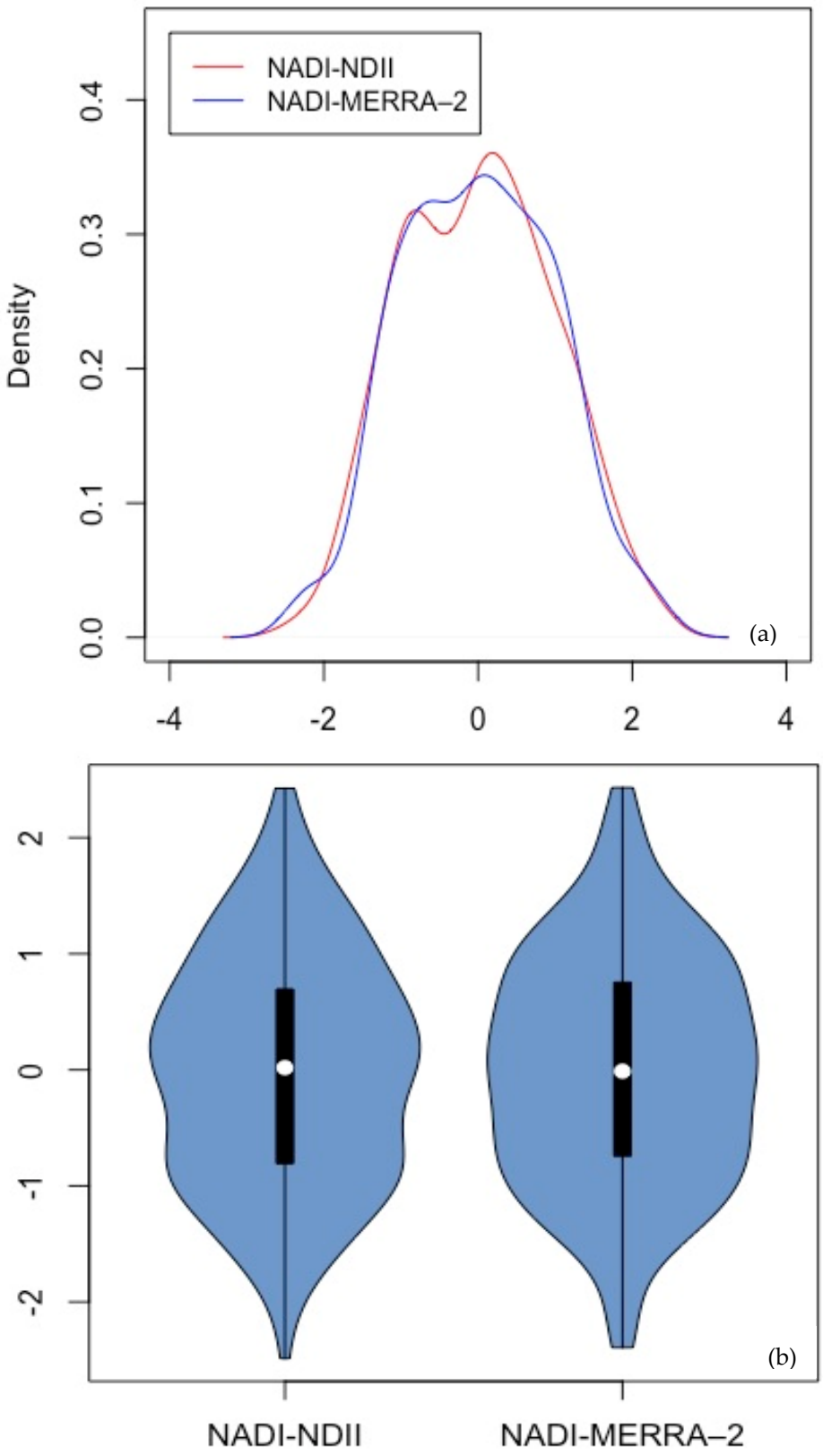

Figure 3. Exploratory data analysis (**a**) Density and (**b**) violin plots for NADI-NDII and NADI-MERRA–2.

Table 2. Summary statistics of NADI-NDII and NADI-MERRA–2.

Index	Min	Max	Mean	Median	STDEV	Variance	Skew.	Kurt.
NADI-NDII	−2.49	2.43	0	0.02	0.986	0.972	0.082	−0.645
NADI-MERRA–2	−2.39	2.43	0	−0.01	0.985	0.969	0.041	−0.513

3.2. NADI Drought Analysis

Figure 4 shows the long-term NADI time series between 1986 and 2016 calibrated with NDII and MERRA–2 root zone soil moisture data including the Nino 3.4 climate index. The NADI indices follow the behaviour of the Nino 3.4 climate index in depicting the wet and dry spells over the study area. Both NADI-NDII and NADI-MERRA–2 managed to depict the major notable droughts events (i.e., 1991/92, 1994/96, 2001/02, and 2014/16 [63–66] in the study area. NADI calibrated with NDII and MERRA–2 data both underestimated the major drought reported in the literature (1991/92 and 2014/16), which were reported as severe and extreme while NADI-NDII characterised these as moderate to severe.

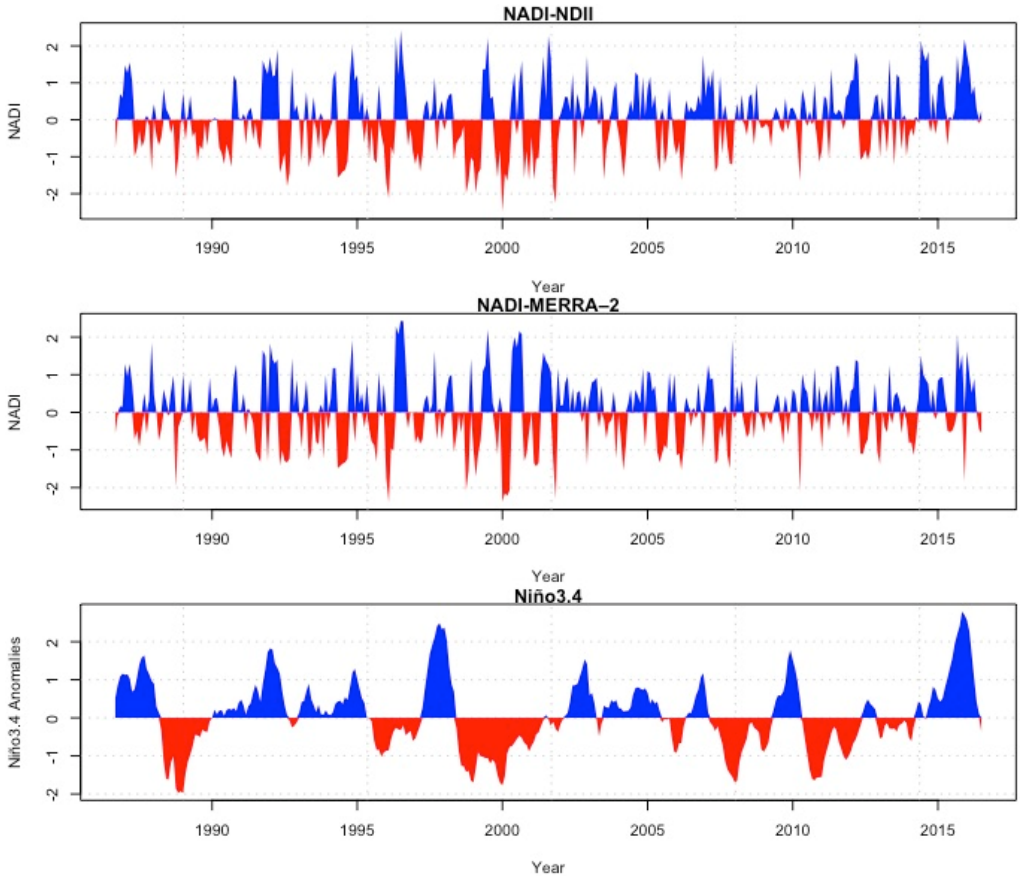

Figure 4. LRC NADI time series showing both the NDII and MERRA–2 soil moisture models including the Nino 3.4 climate index time series between 1986 and 2016.

3.3. Correlation Statistics

Figures 5 and 6 show the correlation between NADI calibrated with NDII and MERRA–2 and the seasonal correlation of the former indices. The correlation coefficient (R^2) between the two indices is 0.58. This shows that a positive relationship exists between the NADI calibrated with NDII and MERRA–2. For the case of seasonal correlation, autumn, spring, winter, and summer reported an R^2 of 0.9, 0.86, 0.61, and 0.15, respectively. The results show that in the summer season, the correlation between the two indices was significantly weak while the autumn was strong.

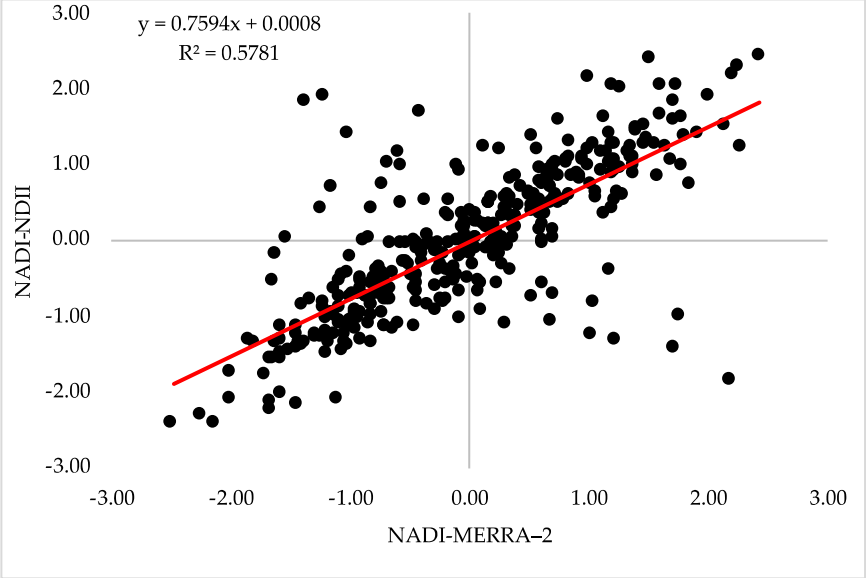

Figure 5. Correlation between NADI-NDII and NADI-MERRA–2 over the Luvuvhu River Catchment between 1986 and 2016.

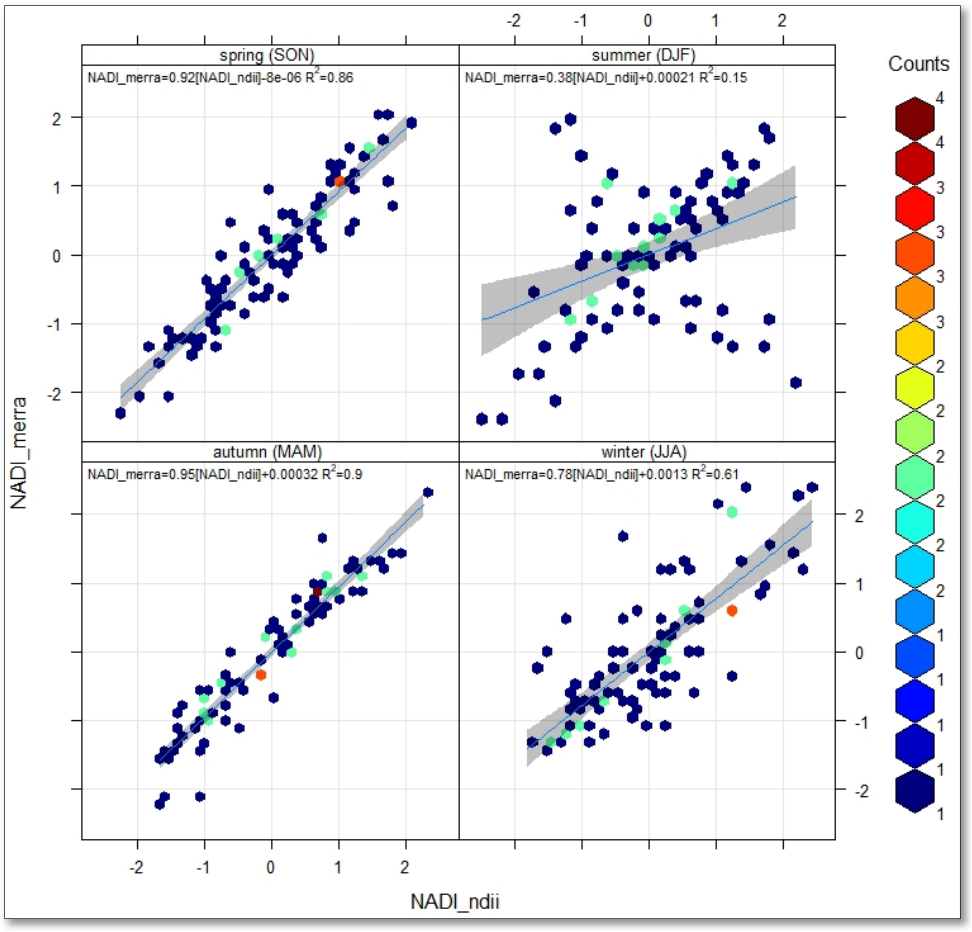

Figure 6. Seasonal correlation of NADI-NDII and NADI-MERRA–2 over the Luvuvhu River Catchment between 1986 and 2016.

The low correlation reported may be influenced by each respective index calibrating variable, for instance, SPI is precipitation based while NADI considers all aspects of the

hydrological cycle and therefore may tend to underestimate events that are highly noted by the SPI. The analysis of variable importance with RF showed that the most important variables influencing NADI-NDII and NADI-MERRA–2 was rainfall with an increasing mean square error (%IncMSE) of more than 25% as shown in Figure 7.

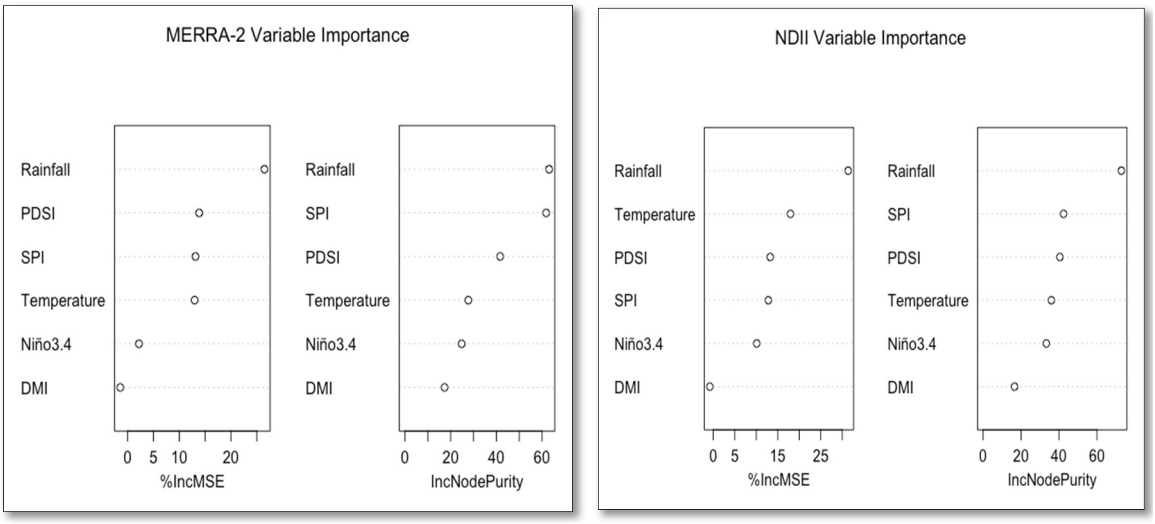

Figure 7. Mean Decrease Accuracy (%IncMSE) and Mean Decrease Gini (IncNodePurity) of attributes as assigned by the random forest for the NADI-MERRA–2 and NADI-NDII.

Figure 8 shows the correlation between NADI (NDII and MERRA–2) and rainfall together with SPI. This is done because rainfall is the most important variable that influences NADI in the study area. Both NDII and MERRA–2 showed weak correlations with rainfall with an R^2 of 0.107 and 0.067, respectively. The same was observed with SPI where although the correlation was week NADI-NDII showed a better correlation compared to NADI-MERRA–2.

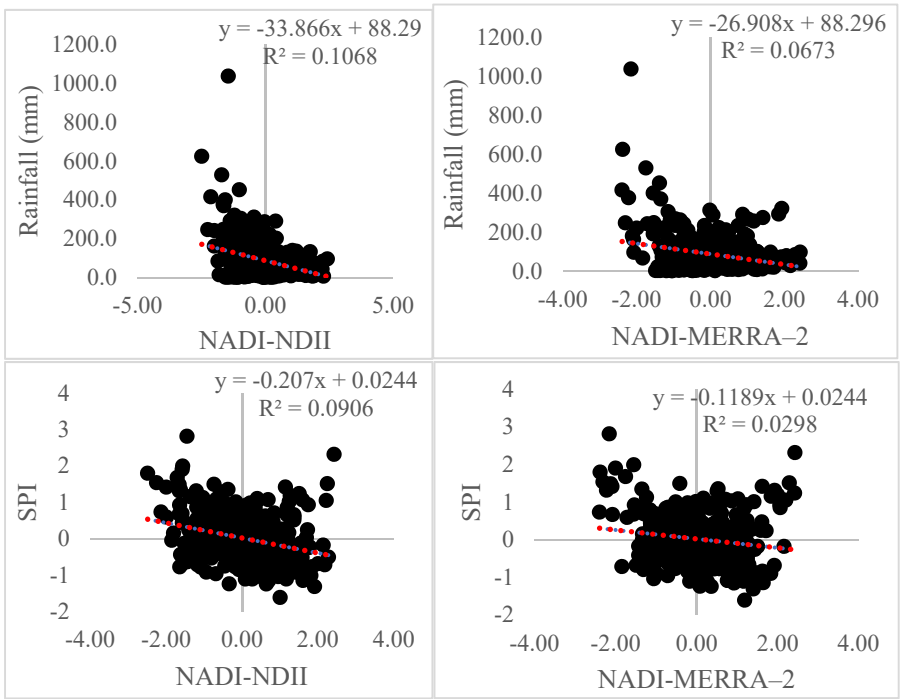

Figure 8. Correlation between NADI (NDII and MERRA–2) time series with SPI and rainfall.

3.4. NADI Trends and Their Significance

The trends analysis and its significance of the NADI time series was also performed in this study. The trend analysis was deduced by fitting the line of best fit in both the NADI-NDII and the NADI-MERRA–2, respectively. The results showed that the indices (NADI-NDII and NADI-MERRA–2 time series) reported a significant positive drought trend at a 95% confidence interval. The smooth linear trend depicted in Figure 9 supports the MK trend results as it shows an increasing positive trend.

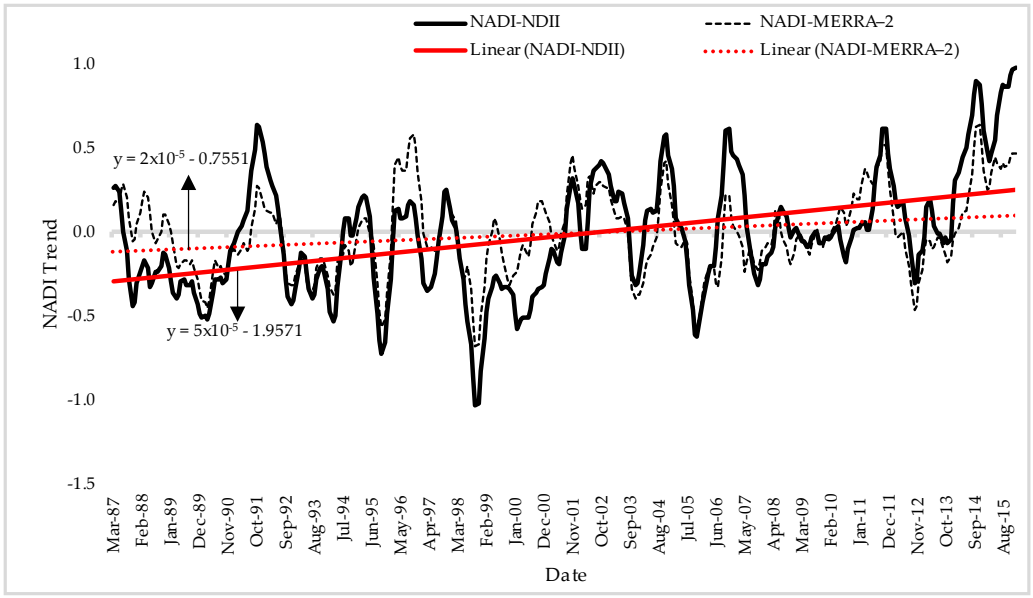

Figure 9. NADI times series and its best fit line for the Luvuvhu River Catchment.

The MK z-scores for NADI-MERRA–2 and NADI-NDII were found to be 1.21 and 2.94, respectively. This, therefore, indicates that NADI-NDII showed a higher degree of deviation from the mean compared to the NADI-MERRA–2. NADI time series trend depicted a decreasing drought trend from the year 2000. There is a notable negative trend that may be attributed to the severe drought that was categorised by both NADI indices in 1986/87 as depicted in Figure 9. However, after the year 2000, the NADI-NDII trend showed to be greater than that of NADI-MERRA–2. Figure 10 shows the LRC NADI sequential MK test results together with the trend slope and magnitude as depicted by the Theil Sen method. The progressive and retrograde series of NADI-NDII (Figure 10a) intersects in September 1990 and from this point until April 2000 the trend showed to be positive. From Figure 10a, it is notable that from February 2000 to May 2014 a negative trend is shown. Figure 9c shows a NADI-MERRA–2 rapid fluctuation between November 1989 and November 2001. During this period, there is an increasing and decreasing trend. Beyond the fluctuation, there is a notable increasing trend between December 2001 and March 2010 which is followed by a decreasing trend between April 2010 and 2014. The period between 2014 and 2016 showed a positive trend. The NADI-NDII showed a significant trend to the level of 0.01 with a magnitude of 0.02 units per annum compared to the NADI-MERRA–2 with a positive trend magnitude of 0.01 units per year.

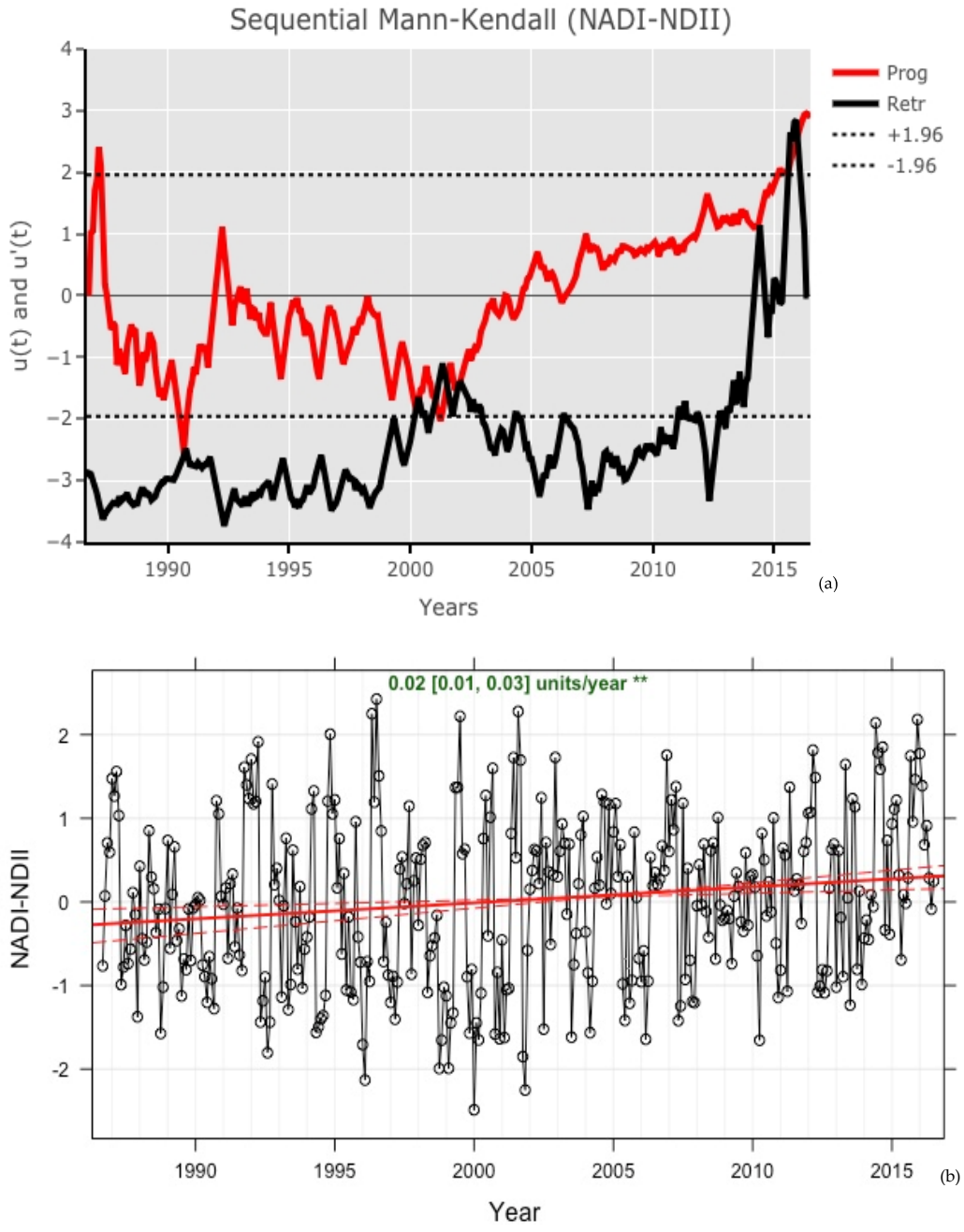

Figure 10. *Cont.*

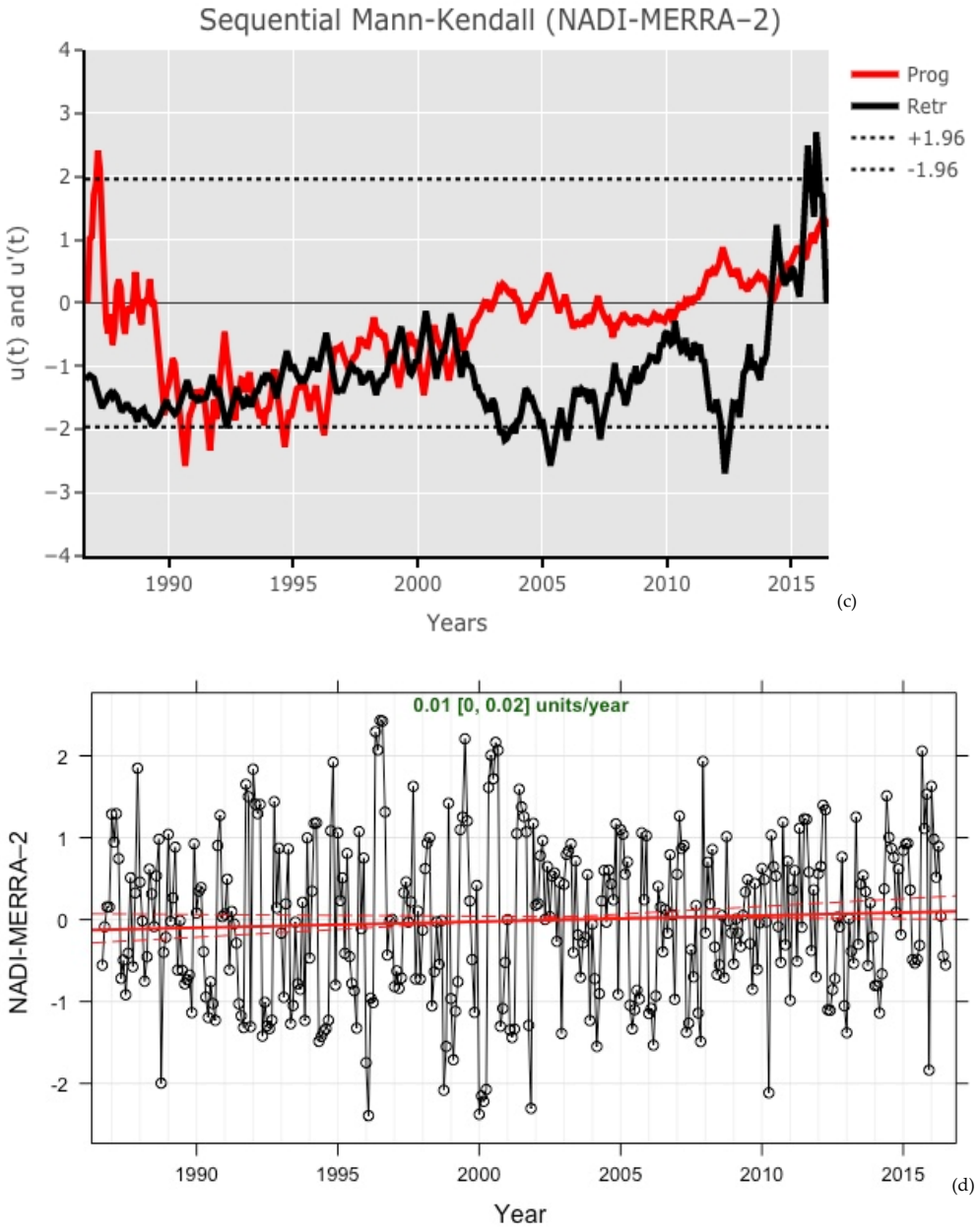

Figure 10. (**a**) SQ-MK trend test for NADI-NDII; (**b**) Theil-Sen trend for NADI-NDII; (**c**) SQ-MK trend test for NADI-MERRA–2; (**d**) Theil-Sen trend for NADI-MERRA–2. The red solid lines indicates the trend estimates and the dashed red lines show the 95% confidence interval. The overall trend for (**b**) is 0.02 units/year and (**d**) is 0.01 units/year, and the 95% confidence interval in the slope is 0.01–0.03 unit/year for (**b**) and 0–0.02 units/year for (**d**). On (**b**), the sign '**' indicates that the trend is significant at the 0.01 level.

3.5. Wavelet Analysis

Figure 11 shows the normalised wavelet power spectrum for NADI-NDII and NADI-MERRA–2 time series from the period of 1986 to 2016. The "u" shaped solid lines in both figures represent the cone of influence (COI) [67]. This is the region of the spectrum that is considered during the analysis. According to [68], COI indicates the area where edge effects occur in the time series. The thick black contour within the COI indicates the 95% significance regions of the confidence interval [61]. Wavelet analysis was used in this study was used to identify dominant variability mode that may be present in the two NADI's calibrated using NDII and MERRA–2. A strong uninterrupted strong power

spectrum was notable between the eighth and 18-month period for NADI-NDII while the NADI-MERRA–2 showed the same between the seventh and 17-month period. These were noted between 1998–2002 and 1994–2001 for NADI-NDII and the NADI-NDII, respectively. The wavelet coherence analysis between NADI-NDII and NADI-MERRA–2 is presented in Figure 12. Wavelet coherence is designed to reveal the coherence and phase lag between two time series as both a function of time and frequency [69]. This approach of time series analysis is good at indicating the teleconnection between two independent time series. The arrows represent a phase relationship, in which case when the arrows pointing to the right indicates a positive phase between two cross-wavelet parameters. An anti-phase is shown by arrows pointing to the left while the upwards or downward arrows show that either of the parameter being analysed is leading (or lagging).

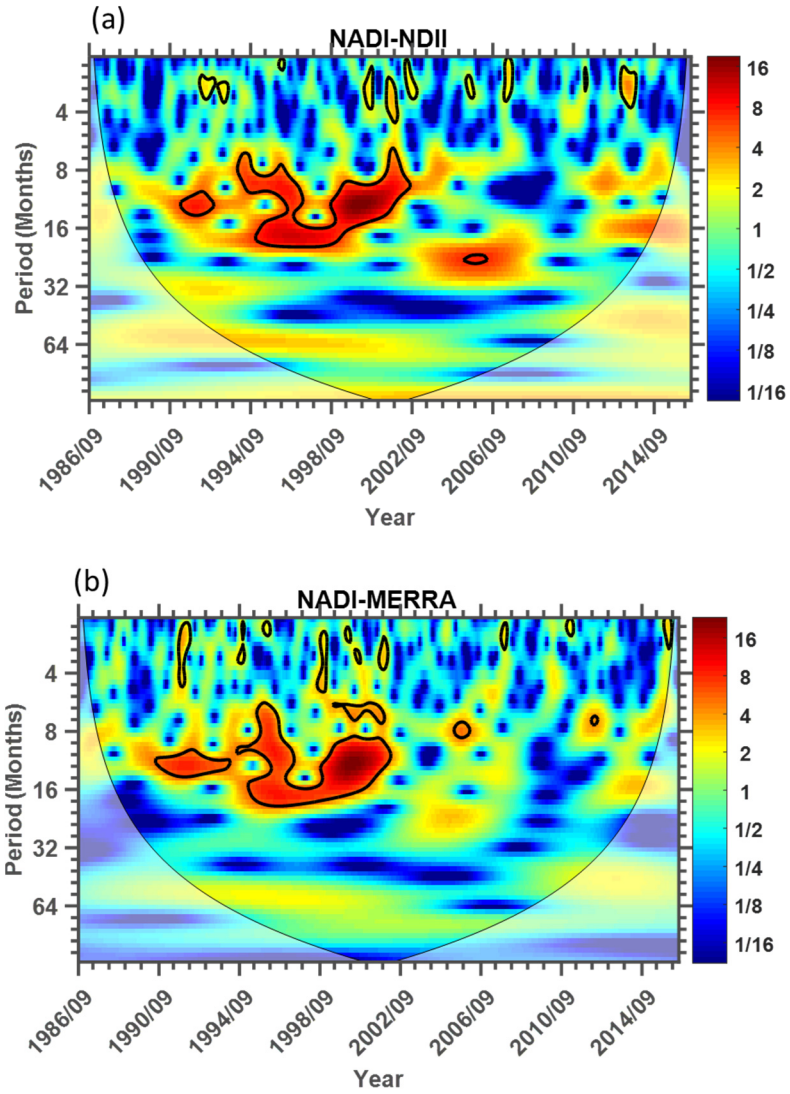

Figure 11. Wavelet transform of (**a**) NADI-NDII and (**b**) NADI-MERRA–2 between 1986 and 2016 in the Luvuvhu River Catchment. The solid black line contour delimits the region (red) where the power is strong and significant, and the cone od influence indicates the 95% confidence interval.

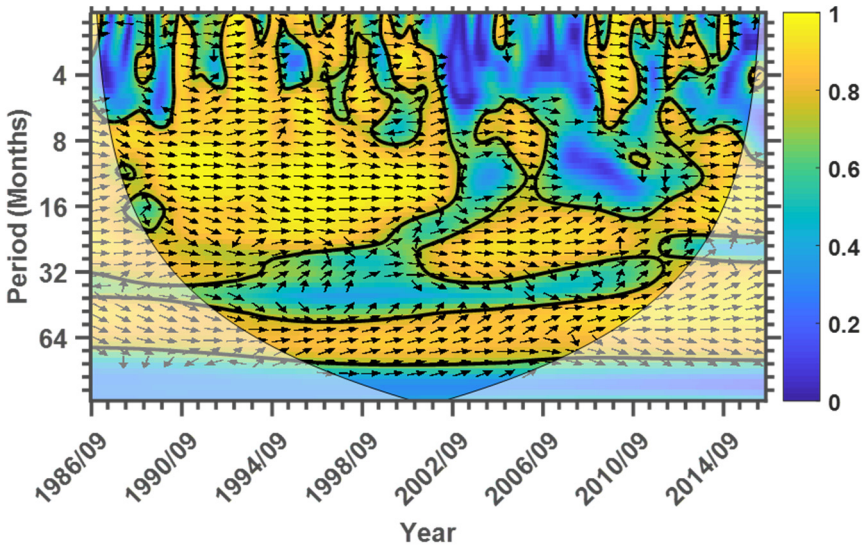

Figure 12. Wavelet coherence between NADI-NDII and NADI-MERRA–2, the phase relationship represented by arrows. The black solid line contour delimits the region (yellow) where the power is string and the cone of influence (solid black line) indicated the 95% confidence level.

Further to the wavelet transform forcings with eight and 18-months and seven and 17-months period for NADI-NDII and NADI-MERRA–2, respectively, wavelet coherence signatures between the two variables were then identified. In general, there is a significant in-phase relationship between NDII and MERRA–2 calibrated NADI at the period band of 6–32 months which is more dominant between the years 1986 and 2002. During this period, 70% of the arrows pointed to the right which is an indication phased relationship. A further uninterrupted significant relationship was observed at the period band of 60–70 months. The study observed that although there are cases where NADI-NDII seems to be leading, majoring of these were in phase with negligible lagging between the NDII and MERRA–2 calibrated NADI. The dominant in-phase relationship between NADI-NDII and NADI-MERRA–2 seems to indicate that both time series can capture almost the same variabilities.

4. Discussions and Conclusions

The NADI-NDII reported three extreme droughts while the NADI-MERRA–2 reported five extreme drought events over the study period. NADI-NDII showed extreme drought conditions in December 1987, October 1988, and February 1996 with the NADI also the value of −2.68, −2.22, and −2.09, respectively. NADI-MERRA–2 showed extreme categories in October 1998 and between January and April 2000. This period coincides with a major flood event reported in the region and drought is not being expected in the region. However, [39] reported that NADI considers a broad perspective of dryness within a catchment rather than just the traditional meteorological drought conditions. Therefore, drought recovery in the catchment was observed as NADI showed severe wet conditions after April 2000. A total of 38.44%, 5.85%, 6.69%, and 0.83% drought events were categorised as mind, moderate, severe, and extreme, respectively by the NADI-NDII. The NADI-MERRA–2 categorised 35.93%, 8.36%, 3.06%, and 1.39% as mild, moderate, severe, and extreme, respectively. Both indices show that the most prominent drought class experiences in the catchment are mild drought or near-normal conditions with less extreme events experienced. Although NADI-MERRA–2 showed 1.39% of extreme drought events, this did not translate to this category frequency. NADI results for both NDII and MERRA–2 were further compared to Nino3.4. Rainfall showed to be the most important variables influencing NADI-NDII and NADI-MERRA–2 with the mean square error of 34% and 27%, respectively. This, therefore, shows that, of all the selected climate indices and meteorological variables, rainfall plays a major role in the development of drought as depicted by NADI which was

used as a drought quantifier in this study. Although drought develops due to below normal average precipitation, a study by [70] reported that when extraordinary droughts form, the probabilities of moderate rain and heavy rain were increased. The MK and Theil-Sen trend showed a positive trend, which indicates that over the study period (1986 to 2016) the LRC was in a recovery state. These trend findings are not consistent with studies that have reported increasing rainfall and temperature trends over north-eastern South Africa by e.g., [71,72]. Studies such as [33] reported a 10-year cyclic increase and decrease in rainfall (between 1931 and 2006) and streamflow (between 1920 and 2006) time series in the LRC. This, therefore, shows that there might also be an interdecadal variation of trend in the NADI time series. Further to this, the results may be attributed to the multivariate nature of the index, as it considers all components of the hydrological cycle and overall catchment water availability.

On the capability of using satellites data as soil moisture proxies, this study has shown that this is possible. The NADI formulated using NDII and MERRA–2 identified some historical droughts that have been experienced in the catchment and further showed an entire catchment drought condition for the LRC. In comparison with available field measured root zone soil moisture between July 2011 and October 2013, MERRA–2 and NDII showed an R^2 of 0. 098 and 0.1036, respectively. Although both show a weak positive relationship, NDII showed a better correlation with the measured in-situ soil rootzone soil moisture compared to the MERRA–2 root zone soil moisture. [39] made use of the Palmer two-layer water budget model to calibrate NADI, however, the same study further indicated that this approach may compromise the quality of the soil moisture data s it assumes a simple relationship between surface and groundwater interaction. Therefore, using satellite data as soil moisture proxies could offer a solution to improve the quality of soil moisture data used in NADI formulation. Although satellites data have their own inherent shortcomings, this study showed that they are useful in monitoring soil moisture as it is often expensive to do so in-situ and long term in-situ soil moisture time series data are limited in many developing nations.

Author Contributions: Conceptualization, F.M.; methodology, F.M. and N.M; formal analysis F.M. and N.M.; data curation, N.M.; writing—original draft preparation, F.M.; writing—review and editing, F.M. and N.M.; visualization, N.M.; formal analysis, F.M. and N.M. All authors have read and agreed to the published version of the manuscript.

Funding: This research received no external funding.

Data Availability Statement: Rainfall and temperature monthly mean data are obtainable from the South African Weather Services on request, streamflow and reservoir storage monthly means are obtainable from the South African Department of Water and Sanitation, https://www.dws.gov.za/Hydrology/Verified/hymain.aspx (accessed on 15 April 2017). MERRA–2 data can be freely downloaded at https://disc.gsfc.nasa.gov/datasets?project=MERRA--2 (accessed on 20 July 2018).

Conflicts of Interest: The authors declare no conflict of interest.

References

1. Wilhite, D.A.; Sivakumar, M.V.; Pulwarty, R. Managing drought risk in a changing climate: The role of national drought policy. *Weather. Clim. Extrem.* **2014**, *3*, 4–13. [CrossRef]
2. Graham, S. Drought: The Creeping Disaster. 2000. Available online: http://earthobservatory.nasa.gov/Features/DroughtFacts/ (accessed on 8 October 2018).
3. Usman, M.T.; Reason, C.J.C. Dry spell frequency and their variability over southern Africa. *Clim. Res.* **2004**, *26*, 199–211. [CrossRef]
4. Mishra, A.K.; Singh, V.P. Drought modeling–A review. *J. Hydrol.* **2011**, *403*, 157–175. [CrossRef]
5. Sriwongsitanon, N.; Gao, H.; Savenije, H.H.G.; Maekan, E.; Saengsawang, S.; Thianpopirug, S. Comparing the Normalized Difference Infrared Index (NDII) with root zone storage in a lumped conceptual model. *Hydrol. Earth Syst. Sci.* **2016**, *20*, 3361–3377. [CrossRef]
6. Feng, H.; Liu, Y. Combined effects of precipitation and air temperature on soil moisture in different land covers in a humid basin. *J. Hydrol.* **2015**, *531*, 1129–1140. [CrossRef]

7. Wang, Y.; Yang, J.; Chen, Y.; Wang, A.; De Maeyer, P. The Spatiotemporal Response of Soil Moisture to Precipitation and Temperature Changes in an Arid Region, China. *Remote Sens.* **2018**, *10*, 468. [CrossRef]
8. Sheffield, J.; Wood, E.F. Global trends and variability in soil moisture and drought characteristics, 1950–2000, from observation-driven simulations of the terrestrial hydrologic cycle. *J. Clim.* **2008**, *21*, 432–458. [CrossRef]
9. Berg, A.; Sheffield, J. Soil Moisture–Evapotranspiration Coupling in CMIP5 Models: Relationship with Simulated Climate and Projections. *J. Clim.* **2018**, *31*, 4865–4878. [CrossRef]
10. Gleick, P.H. Water, drought, climate change, and conflict in Syria. *Weather Clim. Soc.* **2014**, *6*, 331–340. [CrossRef]
11. McKee, T.B.; Doesken, N.J.; Kleist, J. The relationship of drought frequency and duration of time scales. In Proceedings of the Eighth Conference on Applied Climatology, American Meteorological Society, Anaheim, CA, USA, 17–23 January 1993; pp. 179–186.
12. Vicente-Serrano, S.M.; Gouveia, C.; Camarero, J.J.; Beguería, S.; Trigo, R.; López-Moreno, J.I.; Azorín-Molina, C.; Pasho, E.; Lorenzo-Lacruz, J.; Revuelto, J.; et al. Response of vegetation to drought timescales across global land biomes. *Proc. Natl. Acad. Sci. USA* **2012**, *110*, 52–57. [CrossRef] [PubMed]
13. Rouse, J.W.; Haas, R.H.; Schell, J.A.; Deering, D.W. Monitoring vegetation systems in the Great Plains with ERTS. *NASA Spec. Publ.* **1974**, *351*, 309.
14. Palmer, W.C. *Meteorological Drought*; Research Paper. 45; U.S. Weather Bureau: Washington, DC, USA, 1965; p. 58.
15. Shafer, B.A.; Dezman, L.E. Development of a Surface Water Supply Index (SWSI) to Assess the Severity of Drought Conditions in Snowpack Runoff Areas. In Proceedings of the Western Snow Conference, Colorado State University, Fort Collins, CO, USA, April 1982; pp. 164–175. Available online: https://westernsnowconference.org/node/932 (accessed on 13 December 2021).
16. Keyantash, J.A.; Dracup, J.A. An aggregate drought index: Assessing drought severity based on fluctuations in the hydrologic cycle and surface water storage. *Water Resour. Res.* **2004**, *40*, 1–13. [CrossRef]
17. Al Balasmeh, O.; Babbar, R.; Karmaker, T. A hybrid drought index for drought assessment in Wadi Shueib catchment area in Jordan. *J. Hydroinform.* **2020**, *22*, 4. [CrossRef]
18. Hao, Z.; AghaKouchak, A. Multivariate standardised drought index: A parametric multi-index model. *Adv. Water Resour.* **2013**, *57*, 12–18. [CrossRef]
19. Zhu, J.; Zhou, L.; Huang, S. A hybrid drought index combining meteorological, hydrological and agricultural information based on the entropy weight theory. *Arab. J. Geosci.* **2018**, *11*, 1–12. [CrossRef]
20. Barua, S. Drought Assessment and Forecasting Using a Nonlinear Aggregated Drought Index. Ph.D. Thesis, Victoria University, Melbourne, Australia, 2010.
21. McColl, K.A.; Alemohammad, S.H.; Akbar, R.; Konings, A.G.; Yueh, S.; Entekhabi, D. The global distribution and dynamics of surface soil moisture. *Nat. Geosci.* **2017**, *10*, 100. [CrossRef]
22. Koster, R.D.; Dirmeyer, P.A.; Guo, Z.; Bonan, G.; Chan, E.; Cox, P.; Gordon, C.; Kanae, S.; Kowalczyk, E.; Lawrence, D. Regions of strong coupling between soil moisture and precipitation. *Science* **2004**, *305*, 1138–1140. [CrossRef] [PubMed]
23. Brocca, L.; Ciabatta, L.; Massari, C.; Camici, S.; Tarpanelli, A. Soil Moisture for Hydrological Applications: Open Questions and New Opportunities. *Water* **2017**, *9*, 140. [CrossRef]
24. Sheffield, J.; Wood, E.F.; Chaney, N.; Guan, K.; Sadri, S.; Yuan, X.; Olang, L.; Amani, A.; Ali, A.; Demuth, S.; et al. Drought Monitoring and Forecasting System for Sub-Sahara African Water Resources and Food Security. *Bull. Am. Meteorol. Soc.* **2013**, *95*, 861–882. [CrossRef]
25. Dai, A.; Trenbert, K.E.; Qian, T. A global dataset of Palmer Drought Severity Index for 1870–2002: Relationship with soil moisture and effects of surface warming. *J. Hydromet.* **2004**, *5*, 1117–1130. [CrossRef]
26. Furnari, L.; Senatore, A.; De Rango, A.; De Biase, M.; Straface, S.; Mendicino, G. Asynchronous cellular automata subsurface flow simulations in two- and three-dimensional heterogeneous soils. *Adv. Water Resour.* **2021**, *153*, 1–14. [CrossRef]
27. Lopes, D.; Estumano, D.; Macêdo, E.; Quaresma, J. A solution for the Richards equation in layered soil profiles with a single domain approach. *Águas Subterrâneas* **2021**, *35*, 1–11. [CrossRef]
28. De Luca, D.L.; Cepeda, J.M. Procedure to obtain analytical solutions of one-dimensional Richards' equation for infiltration in two-layered soils. *J. Hydrol. Eng.* **2016**, *21*, 04016018. [CrossRef]
29. Ford, T.W.; Harris, E.; Quiring, S.M. Estimating root zone soil moisture using near-surface observations from SMOS. *Hydrol. Earth Syst. Sci.* **2014**, *18*, 139–154. [CrossRef]
30. Hardisky, M.; Klemas, V.; Smart, M. The influence of soil salinity, growth form, and leaf moisture on the spectral radiance of Spartina Alterniflora canopies. *Photogramm. Eng. Remote. Sens.* **1983**, *48*, 77–84.
31. Gelaro, R.; McCarty, W.; Suárez, M.J.; Todling, R.; Molod, A.; Takacs, L.; Randles, C.A.; Darmenov, A.; Bosilovich, M.G.; Reichle, R.; et al. The Modern-Era Retrospective Analysis for Research and Applications, version 2 (MERRA-2). *J. Clim.* **2017**, *30*, 5419–5454. [CrossRef]
32. Reichle, R.H.; Liu, Q.; Koster, R.D.; Draper, C.S.; Mahanama, S.P.; Partyka, G.S. Land surface precipitation in MERRA-2. *J. Clim.* **2016**, *30*, 1643–1664. [CrossRef]
33. Odiyo, J.O.; Makungo, R.; Nkuna, T.R. Long-term changes and variability in rainfall and streamflow in Luvuvhu River Catchment, South Africa. *S. Afr. J. Sci.* **2015**, *111*, 9. [CrossRef]
34. Mzezewa, J.; Misi, T.; van Rensberg, L.D. Characterisation of rainfall at a semi-arid ecotope in the Limpopo Province (South Africa and its implication for sustainable crop production. *Water SA* **2010**, *36*, 19–26. [CrossRef]

35. Hargreaves, G.H.; Samani, Z.A. Reference crop evapotranspiration from temperature. *Appl. Eng. Agric.* **1985**, *1*, 96–99. [CrossRef]
36. Shukla, J.; Mintz, Y. Influence of land surface évapotrans piration on the Earth's climate. *Science* **1982**, *215*, 1498–1501. [CrossRef]
37. Joiner, J.; Yoshida, Y.; Vasilkov, A.P.; Schaefer, K.; Jung, M.; Guanter, L.; Zhang, Y.; Garrity, S.; Middleton, E.M.; Huemmrich, K.F.; et al. The seasonal 572 cycle of satellite chlorophyll fluorescence observations and its relationship to vegetation 573 phenology and ecosystem atmosphere carbon exchange. *Remote. Sens. Environ.* **2014**, *152*, 375–391. [CrossRef]
38. Mbatha, N.; Xulu, S. Time Series Analysis of MODIS-Derived NDVI for the Hluhluwe-Imfolozi Park, South Africa: Impact of Recent Intense Drought. *Climate* **2018**, *6*, 95. [CrossRef]
39. Barua, S.; Ng, A.W.M.; Perera, B.J.C. Drought assessment and forecasting: A case study on the Yarra River catchment in Victoria, Australia. *Aust. J. Water Resour.* **2012**, *15*, 95–108. [CrossRef]
40. Strobl, C.; Boulesteix, A.L.; Kneib, T.; Augustin, T.; Zeileis, A. Conditional Variable Importance for Random Forests. *BMC Bioinform.* **2008**, *9*, 307. [CrossRef] [PubMed]
41. James, G.; Witten, D.; Hastie, T.; Tibshirani, R. *An Introduction to Statistical Learning*; Springer: New York, NY, USA, 2013; Volume 112, p. 18.
42. Meshram, A.; Rai, B. User-Independent Detection for Freezing of Gait in Parkinson's Disease Using Random Forest Classification. *Int. J. Big Data Anal. Healthc.* **2019**, *4*, 57–72. [CrossRef]
43. Yang, L.; Shami, A. On hyperparameter optimization of machine learning algorithms: Theory and practice. *Neurocomputing* **2020**, *415*, 295–316. [CrossRef]
44. Bauer, E.; Kohavi, R. An Empirical Comparison of Voting Classification Algorithms: Bagging, Boosting, and Variants. *Mach. Learn.* **1999**, *36*, 105–139. [CrossRef]
45. Dietterich, T.G. An Experimental Comparison of Three Methods for Constructing Ensembles of Decision Trees: Bagging, Boosting, and Randomization. *Mach. Learn.* **2000**, *40*, 139–157. [CrossRef]
46. Bühlmann, P.; Yu, B. Analyzing Bagging. *Ann. Stat.* **2002**, *30*, 927–961. [CrossRef]
47. Kendall, M.G. *Rank Correlation Methods*; Charles Griffin: London, UK, 1975.
48. Pal, I.; Al-Tabbaa, A. Trends in seasonal precipitation extremes–An indicator of 'climate change' in Kerala, India. Trends in seasonal precipitation extremes–An indicator of 'climate change' in Kerala, India. *J. Hydrol.* **2009**, *367*, 62–69. [CrossRef]
49. Jain, S.K.; Kumar, V. Trend Analysis of Rainfall and Temperature Data for India. *Curr. Sci.* **2012**, *102*, 37–49.
50. Raj, P.P.; Azeez, P.A. Trend analysis of rainfall in Bharathapuzha River basin, Kerala, India. *Int. J. Climatol.* **2012**, *32*, 533–539. [CrossRef]
51. Jain, V.K.; Rivera, L.; Zaman, K.; Espos, R.A.; Sirivichayakul, C.; Quiambao, B.P.; Rivera-Medina, D.M.; Kerdpanich, P.; Ceyhan, M.; Ener, C.; et al. Vaccine for prevention of mild and moderate-to-severe influenza in children. *N. Engl. J. Med.* **2013**, *369*, 2481–2491. [CrossRef]
52. Pohlert, T. Non-Parametric Trend Tests and Change-Point Detection. 2018. Available online: https://cran.r-project.org/web/packages/trend/trend.pdf (accessed on 27 July 2018).
53. Sneyers, S. *On the Statistical Analysis of Series of Observations*; Technical note no. 143, WMO No. 725 415; Secretariat of the World Meteorological Organization: Geneva, Switzerland, 1990; p. 192.
54. Clark, I. *Practical Geostatistics*; Applied Science Publishers: London, UK, 1979.
55. Sayemuzzaman, M.; Jha, M.K. Seasonal and annual precipitation time series trend analysis in North Carolina, United States. *Atmos. Res.* **2014**, *137*, 183–194. [CrossRef]
56. Zelen˘áková, M.; Purcz, P.; Blišt'an, P.; Vranayová, Z.; Hlavatá, H.; Diaconu, D.C.; Portela, M.M. Trends in Precipitation and Temperatures in Eastern Slovakia (1962–2014). *Water* **2018**, *10*, 727. [CrossRef]
57. Theil, H. A rank-invariant method of linear and polynomial regression analysis. In *Henri Theil's Contributions to Economics and Econometrics*; Springer: Dordrecht, The Netherlands, 1992; pp. 386–392.
58. Sen, P.K. Estimates of the regression coefficient based on Kendall's tau. *J. Amer. Statist. Assoc.* **1968**, *63*, 1379–1389. [CrossRef]
59. Yue, S.; Wang, C.Y. Applicability of Prewhitening to Eliminate the Influence of Serial Correlation on the Mann-Kendall Test. *Water Resour. Res.* **2002**, *38*, 4-1–4-7. [CrossRef]
60. Grinsted, A.; Moore, J.C.; Jevrejeva, S. Application of the cross wavelet transform and wavelet coherence to geophysical time series. *Nonlinear Process. Geophys* **2004**, *11*, 561–566. [CrossRef]
61. Torrence, C.; Compo, G.P. A practical guide to wavelet analysis. *Bull. Am. Meteorol. Soc.* **1998**, *79*, 61–78. [CrossRef]
62. Brown, J.D. Statistics corner: Questions and answers about language testing statistics: Skewness and kurtosis. *Shiken* **1997**, *1*, 20–23. Available online: https://www.jalt.org/test/bro_1.htm (accessed on 16 August 1997).
63. FAO. *Drought Impact Mitigation and Prevention in the Limpopo River Basin: A Situation Analysis*; Food and Agricultural Organisation: Rome, Italy, 2004; p. 160.
64. Mason, S.J.; Tyson, P.D. The Occurrence and Predictability of Droughts over Southern Africa. In *Drought Volume 1 A Global Assessment*; Wilhite, D.A., Ed.; Routledge: London, UK, 2000; pp. 113–134.
65. Donnenfeld, A.; Crooke, C.; Hedde, S. *A Delicate Balance: Water Scarcity in South Africa*; Southern Africa Report 13; Institute of Security Studies: Pretoria, South Africa, 2018.
66. Mosase, E.; Ahlablame, L. Rainfall and temperature in Limpopo River Basin, southern Africa: Means, variation and trends from 1979 to 2015. *Water* **2018**, *10*, 364. [CrossRef]

67. Loua, R.T.; Bencherif, H.; Mbatha, N.; Bègue, N.; Hauchecorne, A.; Bamba, Z.; Sivakumar, V. Study on Temporal Variations of Surface Temperature and Rainfall at Conakry Airport, Guinea: 1960–2016. *Climate* **2019**, *7*, 93. [CrossRef]
68. Bilbao, J.; Román, R.; Yousif, C.; Mateos, D.; de Miguel, A. Total ozone column, water vapour and aerosol effects on erythemal and global solar irradiance in Marsaxlokk, Malta. *Atmos. Environ.* **2014**, *99*, 508–518. [CrossRef]
69. Chang, C.; Glover, G.H. Time-frequency dynamics of resting-state brain connectivity measured with fMRI. *NeuroImage* **2010**, *50*, 81–98. [CrossRef]
70. Wang, W.-C.; Chau, K.-W.; Xu, D.-M.; Chen, X.-Y. Improving Forecasting Accuracy of Annual Runoff Time Series Using ARIMA Based on EEMD Decomposition. *Water Resour. Manag.* **2015**, *29*, 2655–2675. [CrossRef]
71. Mckellar, N.; New, M.; Jack, C. Observed and modelled trends in rainfall and temperature for South Africa: 1960–2010. *S. Afr. J. Sci.* **2014**, *110*, 1–13. [CrossRef]
72. Kruger, A.C.; Nxumalo, M.P. Historical rainfall trends in South Africa: 1921–2015. *Water SA* **2017**, *43*, 285–297. [CrossRef]